Journal of Cell Science 109, 1427-1436 (1996)
Printed in Great Britain © The Company of Biologists Limited 1996
JCS3391

Active RNA polymerases are localized within discrete transcription 'factories' in human nuclei

Francisco J. Iborra, Ana Pombo, Dean A. Jackson and Peter R. Cook*

CRC Nuclear Structure and Function Research Group, Sir William Dunn School of Pathology, University of Oxford, South Parks Road, Oxford OX1 3RE, UK

*Author for correspondence (e-mail: peter.cook@path.ox.ac.uk)

SUMMARY

Nascent transcripts in permeabilized HeLa cells were elongated by ~30-2,000 nucleotides in Br-UTP or biotin-14-CTP, before incorporation sites were immunolabelled either pre- or post-embedding, and visualized by light or electron microscopy. Analogues were concentrated in ~2,100 (range 2,000-2,700) discrete sites attached to a nucleoskeleton and surrounded by chromatin. A typical site contained a cluster (diameter 71 nm) of at least 4, and probably about 20, engaged polymerases, plus associated transcripts that partially overlapped a zone of RNA polymerase II, ribonucleoproteins, and proteins rich in thiols and acidic groups. As each site probably contains many transcription units, these results suggest that active polymerases are confined to these sites, which we call transcription 'factories'. Results are consistent with transcription occurring as templates slide past attached polymerases, as nascent RNA is extruded into the factories.

Key words: Nascent RNA, Nuclear compartment, Nuclear speckle, Transcription, RNA polymerase II

INTRODUCTION

Compared with the compartmentation found in the cytoplasm, the nucleus has traditionally been viewed as relatively unstructured. However, recent experiments suggest that nuclei also contain different functional compartments, including 'speckles' rich in splicing components (e.g. Carmo-Fonseca et al., 1991; Carter et al., 1993; for a review, see Spector, 1993) and replication 'factories' where many active DNA polymerases are concentrated (e.g. Nakamura et al., 1986; Hozák et al., 1993). We now investigate whether RNA polymerases are also concentrated in analogous 'factories'.

Although transcripts can be labelled using analogues like [^{3}H]uridine, bromouridine, or Br-UTP, the precise visualization of polymerization sites proves difficult. One problem stems from the rapid rates of elongation (i.e. ~1,400 nucleotides/minute; Shermoen and O'Farrell, 1991) and processing in vivo. [^{3}H]uridine and bromouridine must be transported through membranes, converted into immediate precursors and equilibrated with internal pools before they can be incorporated into nascent RNA; as a result, some transcripts are completed during the labelling period and move away from synthetic sites to accumulate at bottlenecks in the processing pathway. While permeabilization allows direct access of Br-UTP to synthetic sites and control over elongation rates, any unphysiological buffers used could artifactually precipitate nascent transcripts on to underlying structures. A second problem is associated with localizing precisely the incorporated labels; after autoradiography silver grains may be hundreds of nanometers away from incorporated ^{3}H, and immunolabelling gold particles can lie 20 nm away from the Br-RNA they mark (Griffiths, 1993).

In an important series of experiments, Fakan and colleagues localized transcription sites after incubating cells with [^{3}H]uridine for as little as 2 minutes; after autoradiography, they found silver grains over perichromatin fibrils at the edge of condensed chromatin (e.g. Fakan and Puvion, 1980; reviewed by Fakan, 1994; see also Wansink, 1994). Such fibrils are often close to clusters of the interchromatin granules that contain splicing components (Spector, 1993). More recently, 300-500 focal sites where Br-UTP is incorporated have been visualized by immunofluorescence (Jackson et al., 1993; Wansink et al., 1993). It is usually assumed that many tens of thousands of RNA polymerases are active in extranucleolar regions (Chambon, 1974; Cox, 1976) and if these were randomly distributed, a few local concentrations might generate clusters of transcripts that would appear as foci if detection methods were sufficiently insensitive. Alternatively, each focus might truly represent a discrete compartment containing many active polymerases and transcription units. Therefore we devised sensitive procedures to decide which alternative was correct.

In some cases HeLa cells were encapsulated in agarose microbeads (diameter 50-150 μm) to protect them. Next, cells were permeabilized in a 'physiological' buffer that preserves the transcriptional activity of the living cell; this makes it unlikely that the enzymes involved could artifactually aggregate as then they would be expected to lose activity (Jackson et al., 1988). Then nascent RNA chains were elongated by 34-2,070 nucleotides in biotin-CTP or Br-UTP,

before sites containing the analogues were immunolabelled; finally digital images were collected (by both light and electron microscopy) to facilitate quantitative analysis. We find that active RNA polymerases are concentrated in ~2,100 discrete sites with an average diameter of only 71 nm; they do not have the freedom to track throughout euchromatin.

MATERIALS AND METHODS

Encapsulation and lysis

Suspension cultures of HeLa cells were grown, sometimes encapsulated (Jackson and Cook, 1985a) in agarose and regrown for 2 hours, washed twice in PBS, once in 'physiological' buffer (PB; 4°C; Jackson et al., 1988), lysed with saponin (100 μg/ml, 3 minutes; Sigma), washed with PB and used immediately for transcription. PB (pH 7.4) contains 22 mM Na^+, 130 mM K^+, 1 mM Mg^{2+}, <0.3 μM free Ca^{2+}, 32 mM Cl^-, 100 mM CH_3COO^-, 11 mM phosphate, 1 mM ATP, 1 mM dithiothreitol and 0.1 mM phenylmethylsulphonyl fluoride. In the experiments described in Figs 1 and 6, cells were grown for 24 hours in [methyl-^{3}H]thymidine to label their DNA uniformly; this allows precise quantitation of cell number and chromatin removal by electrophoresis (Hozák et al., 1993). For light microscopy, PB contained ribonuclease inhibitor (5 units/ml; Amersham) during washing and lysis.

Transcription in vitro

For Fig. 1 and electron microscopy, encapsulated and lysed cells (10^7/ml) were preincubated (2 minutes, 33°C) in PB before a prewarmed mixture of triphosphates (10× concentrate) was added to give final concentrations of 1.1 mM ATP, 100 μM biotin-14-CTP (Gibco-BRL), GTP and UTP, plus 1.4 mM $MgCl_2$. (1 mM ATP and $MgCl_2$ are present in PB.) For pulse-chases, cells were incubated with biotin-CTP as above, washed 3× in PB and immediately reincubated with a mixture of triphosphates containing 100 μM CTP instead of biotin-CTP. [^{32}P]GTP (250 μCi/ml, ~3,000 Ci/mmol; Amersham) was included in the experiment illustrated in Fig. 1. Transcription was inhibited by adding α-amanitin (Sigma; 20 μg/ml) 10 minutes prior to incubation. After various times at 33°C, reactions were stopped with 10 vols ice-cold PB plus ribonuclease inhibitor (5 units/ml), and beads or cells pelleted. For light microscopy, cells were not encapsulated, 100 μM Br-UTP (Sigma) and CTP were replaced by UTP and biotin-CTP, respectively, and ribonuclease inhibitor (25 units/ml) was present during transcription.

Postembedding immunolabelling for electron microscopy

Sites containing incorporated biotin were immunolabelled using primary and secondary antibodies, and Protein A conjugated with gold particles. After stopping transcription, cells were immediately washed in 50 μg/ml saponin in PB plus ribonuclease inhibitor (5 units/ml), rewashed in PB plus inhibitor, pelleted and fixed (20 minutes, 4°C) in 3% paraformaldehyde and 0.1% glutaraldehyde in PB. After washing successively in Sörensen buffer (SB; 0.1 M Na/K phosphate, pH 7.4), 0.02 M glycine in SB and then SB, cells were dehydrated in ice-cold ethanol, embedded in LR White (polymerization 24 hours at 50°C; London Resin Company) and ultrathin sections on nickel grids immunolabelled. Unspecific binding was blocked by preincubation (30 minutes) in PBS, pH 8.2, with 0.1% Tween-20 and 1% BSA (PBTB buffer). Next, sections were incubated (2 hours) with a monoclonal anti-biotin antibody (5 μg/ml; Sigma) in PBTB, washed in PBS, pH 8.2, incubated (1 hour) with rabbit anti-mouse IgG (1:50 dilution; Jackson labs) in PBTB, rewashed, incubated (1 hour) with Protein A conjugated with 9 nm gold particles (1:100 dilution spun immediately prior to use to remove aggregates; kindly prepared by Mike Hollingshead as described by Griffiths, 1993) in PBTB without Tween and rewashed. Then sections were washed with water, dried, and contrasted with a saturated solution of uranyl acetate in 70% ethanol. In the experiment illustrated in Fig. 5, after immunolabelling and washing, sections were stained using: (i) EDTA regressive stain as described by Clark (1991) without post-staining with lead citrate; (ii) bismuth after blocking amino groups with 1% glutaraldehyde for 15 minutes (Gas et al., 1984); (iii) mercury orange (1 mg/ml from Sigma in 90% ethanol, 30 minutes; Pearse, 1972); or (iv) ruthenium red (0.01% in water, 15 minutes; Erdos, 1986). In the experiment illustrated in Fig. 4, between sectioning and blocking, sections were treated at 37°C (in the order indicated) with RNase A (1 mg/ml in 10 mM Tris-HCl, pH 7.3, 1 hour; Boehringer), Proteinase K (40 μg/ml in PBS, 20 minutes; Boehringer) or RNase H (5 units/ml in 50 mM KCl, 10 mM $MgCl_2$, 1 mM dithiothreitol and 20 mM Hepes-KOH, pH 8.0, 30 minutes). Sections were observed in a Zeiss 912 Omega electron microscope (accelerating voltage 80 kV) and images collected using a CCD camera (1,024×1,024 chip, depth 14 bits).

RNA polymerase II was indirectly immunolabelled using a rabbit antibody directed against RNA polymerase II (Kim and Dahmus, 1986) and goat anti-rabbit IgG conjugated with 15 nm gold particles (1:50 dilution spun immediately prior to use to remove aggregates; BioCell); non-specific labelling was blocked (30 minutes) with 10% foetal calf serum but otherwise conditions were as described above. The polymerase and incorporated biotin were colocalized by immunolabelling transcription sites (as above); then the same face of the LR White section was treated successively with 1% glutaraldehyde (15 minutes), 50 mM NH_4Cl (1 hour) and 10% foetal calf serum (30 minutes) before RNA polymerase II was immunolabelled as above (Griffiths, 1993).

Pre-embedding immunolabelling for electron microscopy

After transcription, encapsulated and lysed cells (5×10^6/ml) were immediately washed with 50 μg/ml saponin in PB, rewashed in PB, incubated (15 minutes at 4°C then 15 minutes at 37°C) with *Eco*RI, *Hae*III and *Alu*I (2,500, 500 and 100 units/ml, respectively) and washed (4°C, 10 minutes) in 0.2% Triton X-100 in PB. For Fig. 6A, the sample was stored for 3 hours at 4°C during which some cut fragments diffused out of the nucleus and 8% chromatin (measured from ^{3}H content) was lost from beads. For Fig. 6B, 88% chromatin was also removed by electroelution (3 hours, 4°C, 3 V/cm; Jackson and Cook, 1985b) in PB. After recovery and washing in PB, both samples of beads were fixed (20 minutes, 4°C) with 4% paraformaldehyde in PB and washed as for post-embedding immunolabelling before non-specific binding was blocked (30 minutes, 20°C) in TBT buffer (20 mM Tris-HCl, 150 mM NaCl, 0.1% BSA, 20 mM Na_3N, 0.005% Tween-20, pH 8.2). Beads were then incubated (2 hours, 20°C) with the anti-biotin antibody (as above) or normal mouse serum (5 μg/ml), washed (3×, 10 minutes) with TBT, incubated with rabbit anti-mouse IgG (as above), rewashed (3× 10 minutes) with TBT, incubated (1 hour, 20°C) with Protein A conjugated with 1 nm gold particles (1:100 dilution in TBT with 0.5% fish gelatine but without Tween-20, spun immediately prior to use to remove aggregates; BioCell), washed successively with TBT (2×), water (3×, HPLC grade) and then with SB. Samples were then postfixed (20 minutes, 20°C) with 2.5% glutaraldehyde in SB, rewashed in SB and then water, silver enhanced using kits (BioCell or Nanoprobes) according to the manufacturers' instructions, stained (1 hour) with 0.5% osmium tetroxide, dehydrated, stained with uranyl acetate and embedded in LR White. PB contained ribonuclease inhibitor at 25, 5 and 0.5 units/ml during incubations with antibodies or restriction enzymes, washing and electrophoresis, respectively.

Immunolabelling for light microscopy

Cryo-sections were prepared using a modification of existing methods (Tokuyasu, 1980; Griffiths et al., 1984; Tooze et al., 1991) which involved washing cells after transcription, fixation, cutting frozen sections (100-200 nm thick) and transferring sections on to coverslips (A. Pombo and P. R. Cook, unpublished). Coverslips were then incubated (1 hour) with a monoclonal anti-Br antibody (20 μg/ml;

Boehringer) in PBS+ (i.e. PBS, 50 mM glycine, 1% BSA and 0.2% fish gelatine, pH adjusted to 7.8 with NaOH), washed 4× in PBS+ over 1 hour, incubated (1 hour) with donkey anti-mouse IgG conjugated with FITC (1:100 dilution in PBS+; Jackson labs), rewashed (10 minutes) in PBS+ and then PBS-0.1% Tween-20, incubated (10 minutes) with 20 μM TOTO-3 (Molecular Probes) in PBS-Tween, washed 2× in PBS-Tween and mounted in Vectashield (Vector Labs). Images were collected on a Bio-Rad MRC 1000 'confocal' microscope (running under Comos software) using the full dynamic range of grey scale and Kalman filtration, incorporated into Adobe Photoshop, 'contrast-stretched', and foci counted without any further processing (i.e. without background subtraction).

Stereology

Analysis of post-embedment (em) sections followed established procedures (Williams, 1977). (1) Collection of 25 images like those in Fig. 2. (2) Measurement (using 'SIS' software) of: (i) the major, 2*x*, and minor, 2*y*, (orthoganol) axes of each cluster; (ii) the area of each cluster; (iii) the numbers of clusters in extra-nucleolar areas; and (iv) the extra-nucleolar area. (3) Calculation (using software kindly supplied by J. Renau-Piqueras) of: (i) the cluster diameter, D, from $D=\sqrt{2}(xy)$; (ii) the mean cluster diameter, D_m, of the Gaussian population using Fullman's formula; (iii) the shape, β, and distribution constant, K; (iv) the mean area, a, and volume, v, of clusters from $v=\beta a^{3/2}$; and (v) finally the number of clusters/unit volume, N_v, using the expression of DeHoff and Rhines. (4) Measurement (after collection of 200 low-power images of nuclei in the same sample using a CCD camera attached to a light microscope and 'Prism' software) of the major and minor nuclear and nucleolar axes, and calculation successively of individual nuclear and nucleolar diameters, mean diameters and volumes, and extra-nucleolar volumes (all as above). Values for pre-embedment (em) sections like those in Fig. 6 were determined as above except that, as cluster diameter roughly equalled section thickness, N_v was calculated using Abercrombie's modification of the expression of DeHoff and Rhines to take into account the Holmes effect. In all cases: (i) sample numbers analysed were greater than the 'minimal sample size' (i.e. within ±10% of the 'progressive mean'); (ii) values for β were 1.41-1.46 (i.e. close to the value for a sphere of 1.38); and (iii) values for K were 1.02-1.39 (i.e. close to a normal distribution).

Images of cryo-sections (as in Fig. 7) were analysed (blind) by three individuals as follows. Extra-nucleolar foci were classified subjectively as 'certain' or 'doubtful' (i.e. those with faint foci or associated with other 'certain' foci) by each individual, and the process repeated for 20 images, which was >'minimal sample size'. Total numbers of foci counted by individuals differed by 14% from the average and 'doubtful' foci constituted <21% of the total; therefore foci were sufficiently distinct to be counted accurately, but this procedure may overestimate numbers of foci by up to 21%. We chose this approach as we were concerned not to underestimate numbers. (Note that automatic counting requires different, but still subjective, assumptions about what constitutes a focus. Consider the 3 clustered foci labelled 3-5 in Fig. 7B, which were counted as 'certain' by all three individuals. They could also be resolved automatically into 3 separate foci by setting an arbitrary threshold well above the average background, but then other 'certain' foci lay below this threshold.) Extranucleolar areas were measured using Adobe Photoshop before N_v was calculated as above, assuming that transcription sites had diameters of 82 nm (Fig. 3C) since it is impossible to determine dimensions of such small structures by light microscopy.

RESULTS

Incorporation of Br-UTP and biotin-CTP by permeabilized cells

After permeabilizing plasma membranes with a weak detergent, encapsulated HeLa cells elongate nascent RNA efficiently under optimal conditions (Jackson et al., 1988). Here we use sub-optimal concentrations of triphosphates to slow elongation so that incorporated label remains close to polymerization sites. We screened various precursors (including Br-UTP, biotin-11-UTP, biotin-14-CTP, fluorescein-12-UTP, coumarin-5-UTP, lissamine-5-UTP and digoxigenin-11-UTP) to see which could be incorporated into RNA and then detected with high sensitivity. Fig. 1 illustrates a typical experiment. Br-UTP (curve 2) was incorporated almost as efficiently as the natural analogue (curve 1), but biotin-14-CTP (curve 3) was incorporated less efficiently. In each case, α-amanitin, an inhibitor of RNA polymerase II, reduced incorporation (e.g. curve 4). 'Pulse-chase' experiments show that biotin-CTP incorporation has no effect on the number of engaged polymerases; for example, after a 'pulse' of biotin-CTP, elongation continues during a 'chase' at the high rate found in controls incubated continuously with the natural analogue (see later). We assume for the sake of discussion that ~35,000 RNA polymerases are active in extra-nucleolar regions in each cell (Chambon, 1974; Cox, 1976; D. A. Jackson and P. R. Cook, unpublished results). Then ~34, 170 and 370 nucleotides would be incorporated during incubations of 1, 5 and 15 minutes with biotin-CTP and most incorporated label should remain in elongating chains. Note that the relative, and not absolute, transcript length is important for our argument, and this is independent of the assumed number of polymerases. Note also that even after long labelling periods it is unlikely that RNA containing the analogues travels far down the processing pathway, as Br-RNA cannot be spliced and biotin-RNA is neither degraded nor chased away from incorporation sites (Wansink et al., 1994; see below).

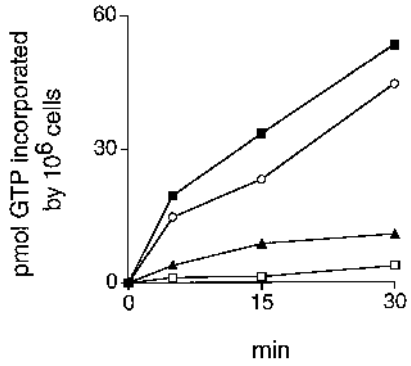

Fig. 1. Elongation rates (measured by incorporation of [^{32}P]GTP into acid-insoluble material) in the presence of: (■) the four natural NTPs; (○) Br-UTP replacing UTP; (▲) biotin-CTP replacing CTP; and (□) biotin-CTP replacing CTP with α-amanitin (20 μg/ml) present for 10 minutes at 4°C prior to, and during, elongation.

Transcription occurs at discrete sites

We next visualized transcription sites in extra-nucleolar regions by electron microscopy. (Hozák et al. (1994) have used a similar approach to visualize nucleolar sites.) Nascent RNA was elongated in biotin-14-CTP for 1, 5 or 15 minutes; after embedding and sectioning, incorporated biotin on the surface of the sections was immunolabelled using primary and secondary antibodies, and then Protein A conjugated to 9 nm gold particles. Immunolabelling particles tended to be

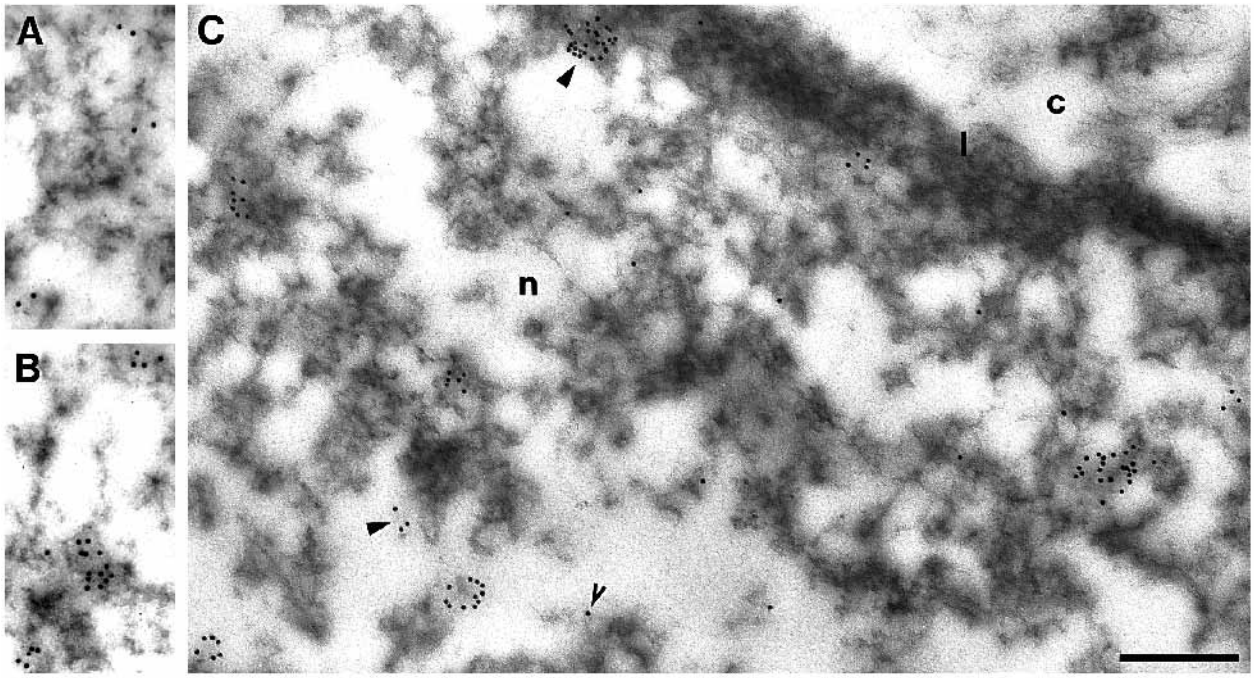

Fig. 2. Visualization of transcription sites. Nascent RNA was elongated in biotin-CTP for (A) 1, (B) 5 and (C) 15 minutes; after cutting sections, incorporated biotin on the surface was immunolabelled with 9 nm gold particles. There are 3, 3 and 9 clusters in A, B and C, respectively. c, cytoplasm; l, lamina; n, nucleus. Closed arrowheads, typical clusters. Open arrowhead, a lone particle. Bar, 250 nm.

clustered (Fig. 2), and the number of particles within a cluster increased with incubation time, which suggested that the clusters marked synthetic sites. Lone particles were scattered over both nucleus and cytoplasm, so they probably resulted from nonspecific, background, binding.

All transcription sites are detected

The impression that clusters marked transcription sites was confirmed by numerical analysis. A cluster was defined as >1 particle lying within 40 nm of another (centre-to-centre distance), and numbers were normalized relative to nuclear area. The numbers of lone particles did not change with time, whereas the numbers in clusters reflected the increase in biotin incorporation (Fig. 3A). Incubation in α-amanitin reduced the number of particles/μm^2 of the section from 9.1±2.7 to 1.2±0.7, and the number of clusters/μm^2 from 0.88±0.2 to 0.31±0.2 (not shown), confirming that labelling reflected transcription. (Note that interchromatin-granule clusters became more obvious after this treatment; Spector et al., 1993.)

This method is sufficiently sensitive to detect all sites. If only a fraction were detected after 1 minute, then increased incorporation should allow previously undetected sites to be detected; however, no more clusters were seen after 5 or 15 minutes (Fig. 3B), despite the increased number of particles in clusters (Fig. 3A). As numbers both of lone particles and clusters remain constant, all incorporation (i.e. transcription) occurs in clusters. Since biotin-CTP is incorporated at one-fifth the rate of CTP, it remained formally possible that the analogue inhibited incorporation into four-fifths of the sites (perhaps because it induced transcripts to terminate prematurely); this possibility can be eliminated because Br-UTP is incorporated almost as efficiently as UTP (Fig. 1) and labels the same total number of sites as biotin-CTP (see below). In any case, transcripts labelled with biotin-CTP do not terminate prematurely, as they can subsequently be elongated normally when the analogue is chased away (see below).

Detection of nascent RNA within polymerization sites

Cluster diameter (i.e. ~75 nm) remained constant despite the increase in transcript length (Fig. 3C, solid line), implying that biotin-RNA was unable to escape from its site of synthesis. This was confirmed using a 5 minute 'pulse' of biotin-CTP followed by a 25 minute 'chase'; the number of particles per cluster (not shown) and cluster diameter (Fig. 3C) remained unchanged, despite the incorporation of ~170 nucleotides during the pulse, and a further ~1,900 nucleotides during the 'chase' (calculated as above). (As biotin-RNA is elongated as efficiently during the 'chase' as the natural transcripts, this also shows that the analogue cannot only be incorporated into a subset of sites.) Surprisingly, nascent transcripts occupy the same small volume despite increasing in length from ~34 (after 1 minute) to ~2,070 nucleotides (during the 'pulse-chase'). This result is difficult to reconcile with models for transcription involving polymerases that track along the template; then the volume occupied by the transcripts should increase roughly in proportion to the length of template transcribed.

Fig. 4 illustrates the expected effects of RNases A and H on a nascent transcript. Some biotin (filled diamonds) is accessible to antibodies and RNase A, but the rest (open diamonds) is obscured by the polymerase and a ribonucleoprotein. Proteinase K treatment uncovers the rest, so that RNase A can now remove all RNA except 23 nucleotides in the transcription 'bubble' (Rice et al., 1991); this, however, can be removed by RNase H. As expected, RNase A reduced the number of immunolabelling gold particles, whereas proteinase K

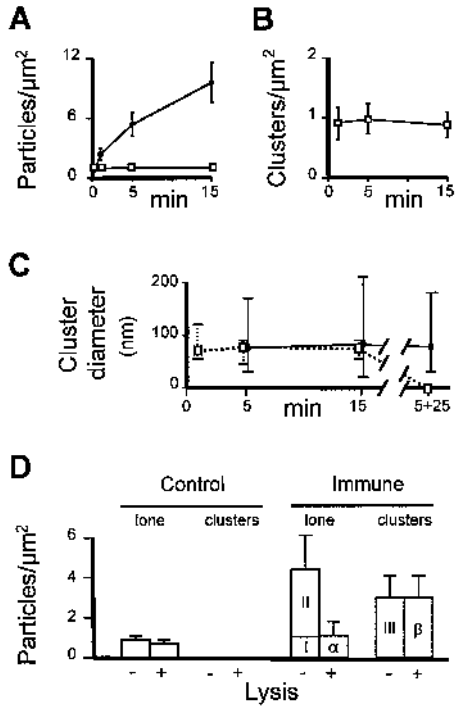

Fig. 3. Nascent transcripts and RNA polymerase II are concentrated in a limited number of discrete sites. (A) Identification of transcription sites. Immunolabelling particles on sections like those illustrated in Fig. 2 were classified either as lone (□) or in clusters (●) (defined as >1 particle lying within 40 nm of another) and the numbers in each category were normalized relative to nuclear area. Some lone particles were found at the beginning, but their number did not change with time; therefore they resulted from non-specific binding. The number in clusters rose with time, reflecting biotin-CTP incorporation. Error bars give s.d.; those for lone particles are obscured by symbols. (B) Incorporation time does not affect the normalized number of clusters (± s.d.). (C) Incorporation time does not affect cluster diameter (bars indicate range). Some sections were untreated (solid lines), whilst others were treated with proteinase K and RNase A, as in Fig. 4D (broken lines). Results for a 5 minute pulse followed by a 25 minute chase are included (no clusters were observed in the treated sample). >50 untreated and 12 treated nuclei were counted at each time; diameters had a normal distribution as Fisher's and the kurtosis coefficient were <0.8 and 2.2-3.7, respectively. (D) Permeabilization does not affect the number of clusters of RNA polymerase II. Encapsulated cells were treated ± saponin, fixed, embedded and thin sections immunolabelled using either a control serum or a serum from a rabbit immunized with RNA polymerase II. The numbers of lone and clustered gold particles were normalized relative to nuclear area. Populations I, II, III, and α and β are discussed in the text. The s.d. is indicated and 11-22 nuclei were analysed.

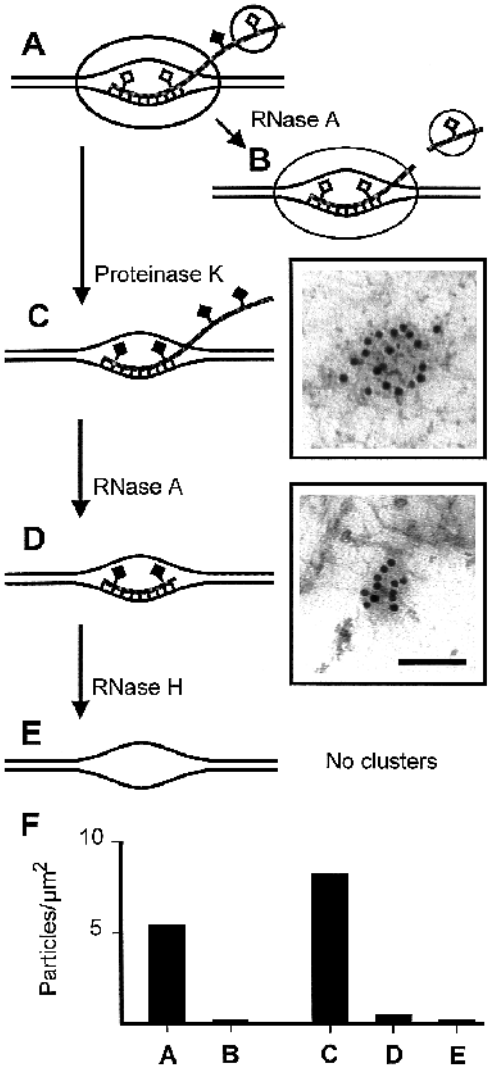

Fig. 4. The effects of RNases on immunodetection. (A) Nascent RNA is shown H-bonded in a transcription 'bubble'; some incorporated biotin (◆) is accessible to antibodies whilst the rest (◇) is obscured by the polymerase and another bound protein. (B) RNase A removes all biotin accessible to antibodies. (C) Proteinase K removes obscuring proteins, increasing the amount of accessible biotin; the micrograph illustrates a typical cluster of gold particles seen after 5 minutes elongation, proteinase K treatment, and immunolabelling as in Fig. 2B. (D) Further treatment with RNase A removes all but H-bonded RNA, which nevertheless contains accessible biotin; the micrograph was prepared as in Fig. 2B. Bar, 100 nm. (E) Subsequent RNase H treatment removes all RNA (and clusters). (F) The number of gold particles (normalized per μm^2) at stages A-E; there were 0.2±0.1 and 0.07±0.05 particles/μm^2 in D and E, respectively.

increased it (Fig. 4F; compare B and C with A). (Proteinase K reduced the number of clusters by 60% (not shown), so it probably removes RNA and protein; therefore, particle numbers before and after proteinase K-treatment should not be compared directly.) Then RNase A again removed all but a few clustered particles (Fig. 4D and F), and two-thirds of these could be eliminated by RNase H to leave a residual background of lone particles (Fig. 4E and F). If the RNA that is sensitive to RNase H is truly bound at a transcription bubble, its length should remain constant irrespective of the amount of synthesis. This turns out to be so. After 1, 5 and 15 minutes incorporation and then treatment with proteinase K and RNase A, the numbers of particles/cluster were 11±5, 9±3 and 12±3, respectively. In each case, two-thirds of the particles in these clusters (i.e. an average of ~7) were again sensitive to RNase H. Moreover, this RNase H-sensitive fraction could be chased out of the bubble (Fig. 3C; sample treated with proteinase K and RNase A, broken lines, 5+25 minutes).

Each engaged polymerase is associated with one bubble, so

the number of RNase H-sensitive particles reflects the number of engaged polymerases in a cluster. Consider biotin moieties tethered through C_{14} linkers (<2 nm long) to ~20 nucleotides (7 nm long) in a bubble. Binding one primary antibody (~9 nm long) to a biotin moiety prevents access of additional antibodies; moreover, the primary antibody is connected, through 1 or 2 secondary antibodies plus protein A, to 2 gold particles (Griffiths, 1993). This means that although a bubble may contain several biotin moieties, only ~2 particles (at most) mark each bubble. Then the ~7 RNase H-sensitive particles/cluster mark ~4 engaged polymerases in the two-dimensional section, and many more than 4 will be packed into a three-dimensional transcription site.

Each cluster of transcription bubbles has an average diameter of 71 nm after proteinase K and RNase A treatment (Fig. 3C). This is an upper limit, as gold particles can lie up to 20 nm away from the associated biotin (Griffiths, 1993).

Incorporation sites contain RNA polymerase II

RNA polymerase II is concentrated in discrete nuclear foci, but it is not known whether these are sites of activity or storage (Wansink, 1994; Bregman et al., 1995). Therefore we simultaneously labelled biotin-RNA with 9 nm particles, as before, and RNA polymerase II with 15 nm particles, using the polyclonal antibody of Kim and Dahmus (1986). Two populations of large particles were seen (Fig. 3D, + lysis). A background of lone particles was also found with a control serum (population α). The second population was probably transcriptionally active (population β); it was clustered (clusters defined as before; diameter 58 nm; range 38-112, $n = 58$) and the number of clusters equalled the number of biotin-containing clusters (Table 1). However, the two types of site did not colocalize exactly; 47% polymerase clusters overlapped a biotin cluster (defined as a particle in one lying within 40 nm of a particle in the other) and the centres of gravity of these overlapping clusters were separated, on average, by ~24 nm (Fig. 5A). Sectioning through polymerase clusters that partially overlapped an equal number of transcript clusters would give such results.

Permeabilization does not affect the number of polymerase II sites

It remained formally possible that lone polymerases aggregated on lysis to give the clusters. Therefore, we analysed the distribution of polymerase II in unlysed cells (Fig. 3D, - lysis). Some lone particles (population II) were found above background (population I), but half the particles were clustered (population III). Lysis reduced the number of lone particles to levels found with a control serum, but did not affect the number of particles in clusters (i.e. populations III and β are similar), the number of clusters (Table 1), or their distribution. As transcriptional activity is retained on lysis, this confirms that lone particles reflect an unbound and inactive pool, while clusters mark bound and active enzyme.

Individual sites can break up to give clusters of smaller sites, for example on exposure to the hypotonic buffers commonly used to isolate nuclei. This can be shown by incorporating biotin-CTP for 15 minutes, incubating samples (10 minutes; 4°C) in the 'physiological buffer' diluted three- or ten-fold in water, before restoring the tonicity and immunolabelling as in Fig. 2C. This increased the number of clusters/μm^2 from 0.86±0.3 to 1.4±0.5 and 1.8±0.5, respectively (i.e. by 1.6 and 2.1 times; not shown). Such lability probably accounts, in part, for the higher density of transcription sites seen by Wansink (1994). If sites also break up in our isotonic buffer, we would overestimate, not underestimate, their number.

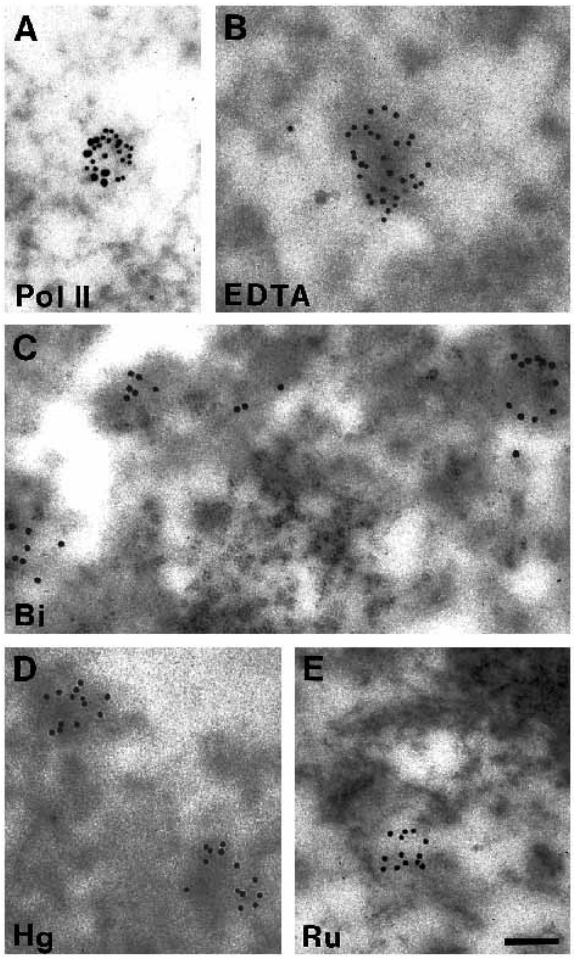

Fig. 5. The architecture of transcription sites. Nascent RNA was elongated in biotin-CTP for 15 minutes, incorporated biotin in transcription sites immunolabelled with 9 nm gold particles, and the sections stained variously. All micrographs are taken at the same magnification (bar, 100 nm). (A) RNA polymerase II was also immunolabelled with 15 nm gold particles prior to staining with uranyl acetate; it is concentrated on one side of the transcription site. (B) EDTA regressive stain; a 'halo' of bleached chromatin surrounds the electron-dense transcription site. (C) Bismuth stains transcription sites (but often not their immediate surroundings) and the cluster of (transcriptionally-inactive) inter-chromatin granules (bottom centre; granule diameter ~25 nm). (D) Mercury orange, a thiol-specific reagent, stains the transcription site. (E) Ruthenium red stains acidic groups in heterochromatin (top right) and regions that overlap, and surround, the transcription site.

The ultrastructure of transcription sites

We next stained transcription sites using various reagents. After regressive staining with EDTA, which bleaches chromatin but not ribonucleoprotein (Clark, 1991), gold particles labelling sites were usually found over dense regions, surrounded by a 'halo' of bleached chromatin (Fig. 5B). Bismuth, which binds to phosphoproteins (e.g. RNA poly-

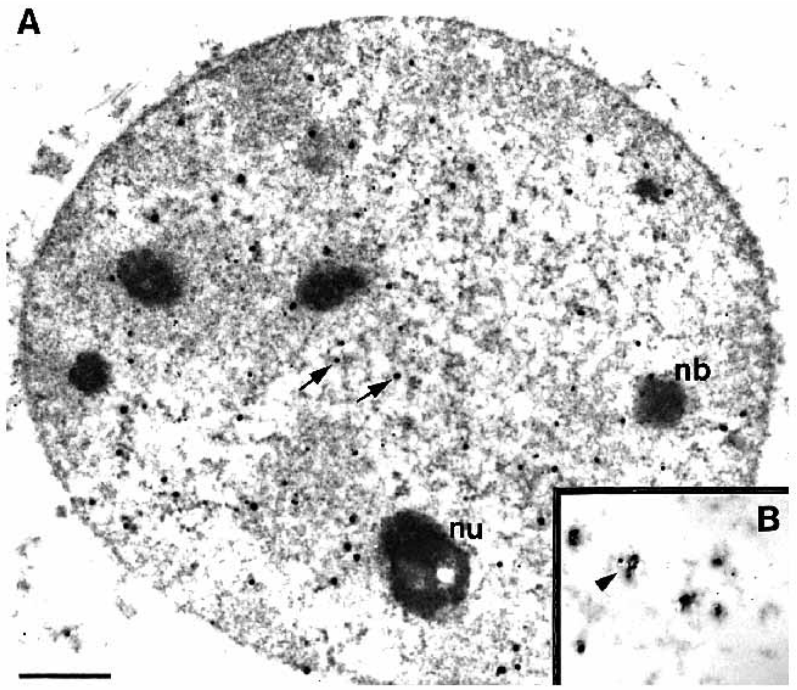

Fig. 6. Transcription sites imaged by pre-embedment immuno-electron microscopy. Encapsulated and permeabilized cells were incubated with biotin-CTP for 15 minutes, chromatin cut with restriction enzymes to 'open' it up, and sites immunolabelled with 1 nm gold particles; gold particles were then enlarged by silver deposition, before embedding and sectioning (thickness, 100 nm). (A) Control sample; 75 transcription sites (marked either by clusters or large silver particles) are distributed throughout the nuclear interior (arrows mark two); there were also 5 sites near remnants of mitochondria. nu, nucleolus; nb, nuclear body. Bar, 1 μm. (B) Sample from which 88% chromatin has been removed by electrophoresis prior to immunolabelling. Sites remain distributed throughout the nucleus (a small region is shown at same magnification as A) despite removal of most chromatin, implying that they are attached to an underlying skeleton. During this procedure, nuclei swell (Table 1) and individual sites fragment to give clusters of enhanced particles (arrowhead).

merase II, RNPs), stained the sites but often not their immediate surroundings (Fig. 5C); sites usually lay several hundreds of nanometers away from clusters of inter-chromatin granules, which were transcriptionally inactive (Spector, 1993). Transcription sites also contained thiols as they could be stained with mercury orange (Fig. 5D). (Many transcription factors (e.g. Sp1, c-jun) contain thiols and their DNA binding is affected by redox levels (e.g. Walker et al., 1993; Ammendola et al., 1994); moreover, glutathione S-transferase, an enzyme involved intimately in thiol metabolism, is found in interchromatin regions; Bennet et al., 1986.) The sites often overlapped, and were immediately surrounded by, regions rich in acidic groups (detected after staining with ruthenium red; Erdos, 1986; Fig. 5E). (Many transcription factors also contain anionic motifs (Earnshaw, 1987) that probably bind this stain.) These results are consistent with chromatin loops forming a 'halo' around two overlapping zones, one rich in transcripts, RNPs and transcription factors, the other rich in RNA polymerase II (Fig. 5A) and additional transcription factors.

The numbers of transcription sites determined by different methods

All the above experiments involved immunolabelling the surface of sections, so we also labelled within sections (i.e. before embedding and sectioning). This has the drawback that access of antibodies and gold particles to their targets is limited by the dense chromatin. Therefore, we first cut chromatin with three restriction enzymes to 'open' it up. (This also detached

Table 1. The number of factories determined by electron (pre- and post-embedment) and light microscopy

	Number clusters or foci (± s.d.)		Nuclear diameter (μm)	Nucleolar diameter (μm)	Nucleoplasmic volume (μm^3)	Total number per nucleus
	per μm^2	per μm^3				
EM, post-embedment						
T sites	0.88±0.2	5.1±2	9.3	3.1	400	2100
Pol II sites	0.9±0.3	5.5±1.7	9.3	3.1	400	2200
Pol II sites (unlysed cells)	1.0±0.3	6.3±2.1	9.2	2.9	400	2500
EM, pre-embedment						
T sites (100 nm)	0.95±0.2	5.8±2	9.1	2.7	380	2200
T sites (200 nm)	2.0±0.6	7.0±2	9.1	2.7	380	2700
T sites (100 nm; eluted)	0.83±0.3	6.1±3	12	6.3	730	4400
T sites (200 nm; eluted)	1.6±0.4	5.0±1	12	6.3	730	3600
LM						
T sites (100 nm)	1.2±0.3	6.6±1.7	9.1	2.7	380	2500
T sites (150 nm)	1.2±0.2	5.3±1.0	9.1	2.7	380	2000
T sites (200 nm)	1.4±0.4	5.1±1.5	9.1	2.7	380	2000

Clusters/foci marking transcription (T) sites or RNA polymerase II (pol II) were counted in sections (thickness of pre-embedment sections indicated) like those illustrated in Figs 2C, 5A, 6 and 7; then numbers were expressed per μm^2 of the two-dimensional image and per unit volume. Nuclear and nucleolar diameters were also measured in the same sections and used to derive extra-nucleolar (nucleoplasmic) volumes, and so the total number of extra-nucleolar clusters/foci per nucleus.

88% of the length of chromatin loops from the underlying skeleton (see below); as a result, many released fragments diffused out of nuclei and 8% of total chromatin was lost from beads; not shown.) Next, sites containing incorporated biotin were labelled using primary and secondary antibodies, and then Protein A conjugated with 1 nm gold particles. As such particles are difficult to see by electron microscopy, they were enlarged by silver deposition before embedding and sectioning.

The resulting sections contained three populations of enlarged particles (Fig. 6A). One population of lone particles (diameter ~10 nm), which cannot be seen at this magnification, was scattered throughout the sample and so was derived by enlargement of an inevitable background of 1 nm particles; it was also found with a control antibody (not shown). The second population contained clusters of such ~10 nm particles (defined as before). A third population of (larger) lone particles (minimum and average diameters 50 and 126 nm, respectively) was clearly derived as individuals in a cluster fused together. The last two populations marked transcription sites as: (i) they were only seen using biotin-CTP and the specific first antibody; and (ii) the size of bigger particles increased with increased transcription and was reduced by α-amanitin (not shown).

Sites in unencapsulated cells were also visualized using a completely independent method. Nascent chains were elongated by ~1,100 nucleotides in Br-UTP (Fig. 1), fixed, cryo-sections (100, 150 or 200 nm thick) prepared and indirectly immunolabelled using a fluorescently-tagged antibody. Many discrete foci marking transcription sites were then visible by light microscopy (Fig. 7A). No such foci were seen in unpermeabilized cells, and their intensity in permeabilized cells was reduced or abolished by treatment with α-amanitin and RNase A, respectively (not shown; see also Jackson et al., 1993). Physical, as opposed to optical, sectioning ensures that the background in the resulting images is low (Fig. 7B), enabling accurate counting. However, the low resolution of light microscopy means that individual sites appear aberrantly large (diameters ~300 nm), inevitably giving the impression that nascent transcripts occupy a much larger volume.

The numbers of clusters/foci per nucleus were calculated using the appropriate stereological techniques, which included corrections for the numbers on the edge of sections and nucleolar volumes, from the densities measured in the two or three dimensions of these various sections (Table 1). Numbers determined using one method but sections of different widths were gratifyingly similar, as were those obtained using different methods.

Transcription sites are attached to a nucleoskeleton

Finally, we showed by electron microscopy that transcription sites were attached to a nucleoskeleton. After incorporating biotin and treatment with restriction enzymes, 88% chromatin was removed electrophoretically to leave residual fragments attached to an underlying skeleton (Jackson and Cook, 1988; Hozák et al., 1995); then sites were marked by silver enhancement as before. If sites were not attached to an underlying structure, they should either elute from beads or, if too large, they should move under the influence of the field to the edge of nuclei. However, sites remained distributed throughout nuclei and their numbers even increased, probably because the sites fragment into 'clusters of clusters' during the lengthy procedure (Fig. 6B, Table 1).

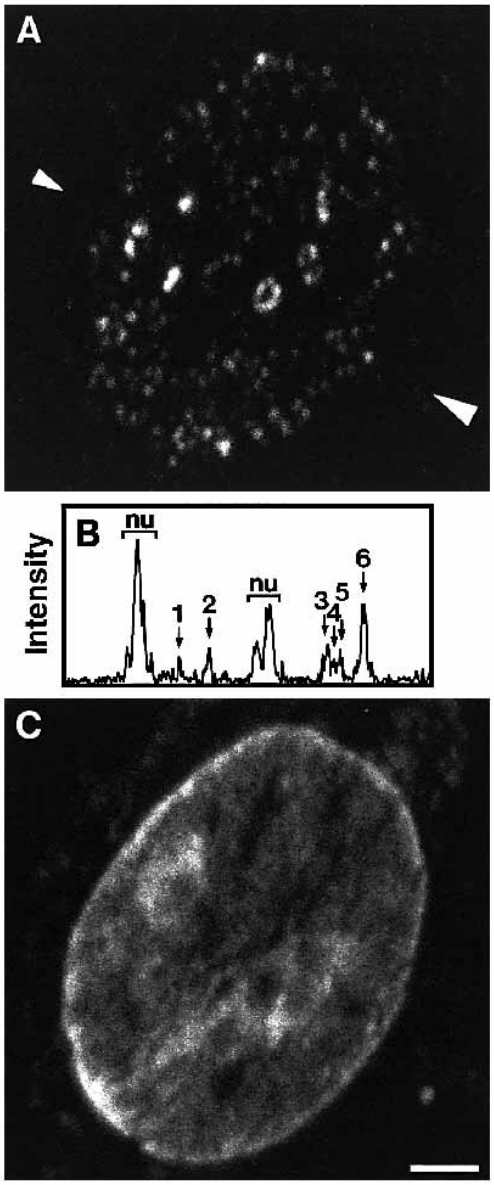

Fig. 7. Transcription sites imaged by light microscopy. Permeabilized cells were incubated with Br-UTP for 15 minutes, cryo-sections (100 nm thick) prepared and Br-RNA immunolabelled with fluorescein (nucleic acids were counterstained with TOTO-3). Green and far-red images of one section were collected sequentially and are shown without further background subtraction or digital processing. (A) Transcription sites (green channel). Three individuals counted (blind) 126, 146 and 148 extra-nucleolar foci in this image. Nucleolar foci are often crescent shaped (as here); mitochondrial foci in the cytoplasm are also occasionally seen. (B) The fluorescence intensity (scale 0-255) along a line, from small to large arrowhead in (A), passing through 6 extra-nucleolar foci; all appear as discrete peaks above the background. nu, nucleolar foci. (C) Nucleic acids (far-red channel). Bar, 2.5 μm.

DISCUSSION

Different methods for visualizing extra-nucleolar transcription sites

Sites were directly visualized using three sensitive methods.

(Note that we distinguish between active transcription units and sites, as an individual site may contain many transcription units and engaged polymerases.) In all cases, HeLa cells were permeabilized in a 'physiological' buffer to preserve as much nuclear structure and function as possible, and digital images were collected to facilitate numerical analysis. In the first method, cells were encapsulated in agarose microbeads to protect them during subsequent manipulation, permeabilized, and nascent RNA chains elongated by 30-2,000 nucleotides in biotin-14-CTP; after embedding and sectioning, incorporated biotin on the surface of sections was immunolabelled with gold particles. Most extra-nucleolar particles lay in small clusters (Fig. 2) which marked nascent RNA because the average number of particles in a cluster rose as more biotin was incorporated, and fell after treatment with α-amanitin or RNase A (e.g. Fig. 4F). We feared that biotinylated RNA might move quickly to distant processing sites, but found none could be chased away (Fig. 3C, solid line); presumably biotin-RNA, like Br-RNA (Wansink et al., 1994), cannot be processed. Some particles were bound to biotin-RNA that was still H-bonded to the template as they could be removed by RNase H (Fig. 4F); they marked 4 or more engaged polymerases packed together into structures with average diameters of, at most, 71 nm (Fig. 3C, solid line). This method proved sufficiently sensitive to allow visualization of nascent RNA in transcription 'bubbles' (Fig. 4), as well as detection of all sites; if only a fraction had been detected, increased incorporation should have increased the number seen, but it did not (Fig. 3B). Therefore, it provides the most accurate estimate of site number and size.

The second method involved immunolabelling before, and not after, embedding. Biotin-CTP was incorporated as above and then access of antibodies and gold particles to the nuclear interior was improved by 'opening' chromatin by cutting it with restriction enzymes. After immunolabelling with 1 nm gold particles, bound particles were enlarged by silver deposition so that they now marked sites throughout the resulting sections (Fig. 6A).

Sites were also visualized in unencapsulated cells by light microscopy. Modern 'confocal' microscopes have a resolution of ~200, ~200 and ~500 nm in the *x,y* and *z* axes, respectively, which makes quantitation of small sites difficult. Although resolution can be improved by digitally deconvoluting information from serial sections, this brings attendant problems (e.g. see Shaw et al., 1992), so we physically cut our samples into sections that were 100-200 nm thick. Here, nascent chains were elongated by ~1,100 nucleotides in Br-UTP before samples were fixed, cryo-sectioned and sites containing incorporated Br indirectly immunolabelled; fluorescent foci then marked sites throughout the sections (Fig. 7). Physical, as opposed to optical, sectioning ensures low backgrounds and enables accurate counting, but the poor resolution inevitably means that individual sites appear aberrantly large, encouraging the impression that nascent transcripts occupy a larger volume than they actually do.

Sites containing RNA polymerase II were also immunolabelled to provide a fourth, indirect, method of marking transcription sites (Fig. 5A; Table 1). Two populations of enzyme were seen. One, marked by lone gold particles, was diffusely spread; it lay remote from incorporation sites and so was inactive. The other, marked by clusters of gold particles, overlapped the incorporation sites; therefore it includes the active enzymes. This method allowed us to eliminate the possibility that lone polymerizing complexes were aggregating on lysis; although our methods clearly affect nuclear volume and ultrastructure (e.g. Table 1), unlysed cells contained the same number and distribution of polymerase II clusters (Fig. 3D; Table 1). Aggregation is unlikely after lysis, because the three other methods gave similar results despite differing in all subsequent steps (e.g. in the use of agarose microbeads and analogues, immunolabelling procedures, embedding techniques, imaging and stereology).

There are only ~2,100 transcription sites per nucleus

The numbers of sites (i.e. 2,000-2,700; best estimate 2,100) determined using the four methods were gratifyingly similar (Table 1). Such a low number cannot result from the failure of many other (unseen) sites to incorporate the analogues, as Br-UTP is polymerized almost as efficiently as UTP (Fig. 1). Most surprisingly, nascent transcripts occupied the same small volume despite a sixtyfold increase in elongation.

While our results generally differ quantitatively from those obtained previously, they do not differ qualitatively. For example, transcription sites have been localized by autoradiography to the perichromatin fibrils that lie close to clusters of interchromatin granules at the edge of condensed chromatin (reviewed by Fakan, 1994; see also, Wansink, 1994); we find an essentially similar location. ~500 discrete sites were also visualized by immunofluorescence (Jackson et al., 1993; Wansink et al., 1993) and the higher numbers seen here are almost certainly due to improved sensitivity and resolution. We also confirm that most RNA polymerase II is found in 'speckles' (Wansink, 1994; Bregman et al., 1995; Fig. 5A) and that transcription sites are closely associated with an underlying skeleton (e.g. Jackson et al., 1993; Wansink et al., 1993).

Mechanisms of transcription

How does the number of sites relate to the number of active polymerases and transcription units? Although it is widely assumed that 25,000-100,000 polymerases are active at any one time, the evidence for this assumption is indirect (Chambon, 1974; Lewin, 1975; Cox, 1976). Therefore, it remains possible that only ~2,100 transcription units (and even fewer genes) are active in a sub-tetraploid HeLa nucleus; then each site would contain one unit. However, it seems unlikely that so few genes can be active or that each of our methods is sufficiently sensitive to detect all (individual) transcription units.

Alternatively, many transcription units might be packed into each of the ~2,100 sites. In this case, our methods could be less sensitive, but still able to detect all sites because each site contained many units and perhaps 20 active polymerases. This attractive alternative is, however, difficult to reconcile with the model for transcription found in most textbooks that involves a polymerase that moves along the template (e.g. Alberts et al., 1994). Some mechanism must corral such tracking polymerases into a site with an average diameter of 71 nm, and it is difficult to imagine what that might be. One way of doing so is to tie the templates in very short loops to the nucleoskeleton, but then cutting those loops with restriction enzymes should allow the associated polymerases and transcripts to elute, but it does not (Fig. 6B; Table 1; Jackson et al., 1993). Importantly, we would expect tracking polymerases

to generate transcripts that occupied a volume that increased in rough proportion to the length of the transcribed template, but this volume, reflected by cluster diameter, remains unchanged as transcripts become sixtyfold longer (Fig. 3C, broken lines).

A variant of this alternative involving many transcription units per site is consistent with all our results; it requires that transcription occurs as the template moves past the fixed enzyme, rather than vice versa (Jackson et al., 1981; Cook, 1994). Each site, or 'factory', would be attached to the nucleoskeleton and surrounded by a 'halo' of chromatin loops. It would contain three zones: one rich in polymerases, which overlaps another containing nascent RNA, which, in turn, abuts a processing area (see also Carmo-Fonseca et al., 1991; Carter et al., 1993). These zones would be analogous to the fibrillar centre, dense fibrillar component and the granular component of nucleolar transcription factories (Spector, 1993; Hozák et al., 1994). Each factory would be associated with many different transcription units, and transcripts would be extruded into the constant volume of the transcript zone as the units slid past.

We thank the Cancer Research Campaign, the Wellcome Trust and the Junta Nacional de Investigação Científica e Tecnológica (Portugal) for support; Drs M. Hollingshead, M. E. Dahmus, J. Renau-Piqueras and Mr M. Lloyd for kindly supplying reagents or software; and Dr D. Vaux and Mr J. Sanderson for their help.

REFERENCES

Alberts, B., Bray, D., Lewis, J., Raff, M., Roberts, K. and Watson, J. D. (1994). *Molecular Biology of the Cell*, 3rd edn. Garland, New York.

Ammendola, R., Mesuraca, M., Russo, T. and Cimino, F. (1994). The DNA-binding efficiency of Sp1 is affected by redox changes. *Eur. J. Biochem*. **225**, 483-489.

Bennet, C. F., Spector, D. L. and Yeoman, L. C. (1986). Nonhistone protein BA is a glutathione S-transferase localized to interchromatinic regions of the cell nucleus. *J. Cell Biol*. **102**, 600-609.

Bregman, D. B., Du, L., van der Zee, S. and Warren, S. L. (1995). Transcription-dependent redistribution of the large subunit of RNA polymerase II to discrete nuclear domains. *J. Cell Biol*. **129**, 287-298.

Carmo-Fonseca, M., Tollervey, D., Pepperkok, R., Barabino, S. M. L., **Merdes, A., Brunner, C., Zamore, P. D., Green, M. R., Hurt, E. and Lamond, A. I.** (1991). Mammalian nuclei contain foci which are highly enriched in components of the pre-mRNA splicing machinery. *EMBO J.* **10**, 195-206.

Carter, K. C., Bowman, D., Carrington, W., Fogarty, K., McNeil, J. A., Fay, F. S. and Lawrence, J. B. (1993). A three-dimensional view of precursor messenger RNA metabolism within the nucleus. *Science* **259**, 1330-1335.

Chambon, P. (1974). RNA polymerases. In *The Enzymes*, vol. 10 (ed. P. D. Boyer), pp. 261-331. Academic Press, New York.

Clark, M. W. (1991). Nucleolar-specific positive stains for optical and electron microscopy. *Meth. Enzymol*. **194**, 717-728.

Cook, P. R. (1994). RNA polymerase: structural determinant of the chromatin loop and the chromosome. *BioEssays* **16**, 425-430.

Cox, R. F. (1976). Quantization of elongating form A and B RNA polymerases in chick oviduct nuclei and effects of estradiol. *Cell* **7**, 455-465.

Earnshaw, W. C. (1987). Anionic regions in nuclear proteins. *J. Cell Biol*. **105**, 1479-1482.

Erdos, G. W. (1986). Localization of carbohydrate-containing molecules. In *Ultrastructural Techniques for Microorganisms* (ed. H. C. Aldrich and W. J. Todd), pp. 399-416. Plenum Press, New York, London.

Fakan, S. and Puvion, E. (1980). The ultrastructural visualization of nuclear and extranucleolar RNA synthesis and distribution. *Int. Rev. Cytol*. **65**, 255-299.

Fakan, S. (1994). Perichromatin fibrils are *in situ* forms of nascent transcripts. *Trends Cell Biol*. **4**, 86-90.

Gas, N., Inchauspe, G., Azum, M. and Stevens, B. (1984). Bismuth staining of a nucleolar protein. *Exp. Cell Res*. **151**, 447-457.

Griffiths, G., McDowall, A. W., Back, R. and Dubochet, J. (1984). On the preparation of cryosections for immunocytochemistry. *J. Ultrastruct. Res*. **89**, 65-78.

Griffiths, G. (1993). *Fine Structure Immunocytochemistry*. Springer-Verlag, Berlin, Heidelberg.

Hozák, P., Hassan, A. B., Jackson, D. A. and Cook, P. R. (1993). Visualization of replication factories attached to a nucleoskeleton. *Cell* **73**, 361-373.

Hozák, P., Cook, P. R., Schöfer, C., Mosgöller, W. and Wachtler, F. (1994). Site of transcription of ribosomal RNA and intra-nucleolar structure in HeLa cells. *J. Cell Sci*. **107**, 639-648.

Hozák, P., Sasseville, A. M.-J., Raymond, R. and Cook. P. R. (1995). Lamin proteins form an internal nucleoskeleton as well as a peripheral lamina in human cells. *J. Cell Sci*. **108**, 635-644.

Jackson, D. A., McCready, S. J. and Cook, P. R. (1981). RNA is synthesised at the nuclear cage. *Nature* **292**, 552-555.

Jackson, D. A. and Cook, P. R. (1985a). A general method for preparing chromatin containing intact DNA. *EMBO J*. **4**, 913-918.

Jackson, D. A. and Cook, P. R. (1985b). Transcription occurs at a nucleoskeleton. *EMBO J*. **4**, 919-925.

Jackson, D. A. and Cook, P. R. (1988). Visualization of a filamentous nucleoskeleton with a 23 nm axial repeat. *EMBO J*. **7**, 3667-3677.

Jackson, D. A., Yuan, J. and Cook, P. R. (1988). A gentle method for preparing cyto- and nucleo-skeletons and associated chromatin. *J. Cell Sci*. **90**, 365-378.

Jackson, D. A., Hassan, A. B., Errington, R. J. and Cook, P. R. (1993). Visualization of focal sites of transcription within human nuclei. *EMBO J*. **12**, 1059-1065.

Kim, W.-Y. and Dahmus, M. E. (1986). Immunocytochemical analysis of mammalian RNA polymerase II subspecies: stability and relative in vivo concentration. *J. Biol. Chem*. **261**, 14219-14225.

Lewin, B. (1975). Units of transcription and translation: sequence components of heterogeneous nuclear RNA and messenger RNA. *Cell* **4**, 77-93.

Nakamura, H., Morita, T. and Sato, C. (1986). Structural organisation of replicon domains during DNA synthetic phase in the mammalian nucleus. *Exp. Cell Res*. **165**, 291-297.

Pearse, A. G. E. (1972). *Histochemistry: theoretical and applied*. Third edition, vol. 2. Churchill Livingstone, Edinburgh and London.

Rice, G. A., Kane, C. M. and Chamberlin, M. J. (1991). Footprinting analysis of mammalian RNA polymerase II along its transcript: an alternative view of transcriptional elongation. *Proc. Nat. Acad. Sci. USA* **88**, 4245-4249.

Shaw, P., Highett, M. and Rawlings, D. (1992). Confocal microscopy and image processing in the study of plant nuclear structure. *J. Microsc*. **166**, 87-97.

Shermoen, A. W. and O'Farrell, P. H. (1991). Progression of the cell cycle through mitosis leads to abortion of nascent transcripts. *Cell* **67**, 303-310.

Spector, D. L. (1993). Macromolecular domains within the cell nucleus. *Annu. Rev. Cell. Biol*. **9**, 265-315.

Spector, D. L., O'Keefe, R. T. and Jiménez-García, L. F. (1993). Dynamics of transcription and pre-mRNA splicing within the mammalian cell nucleus. *Cold Spring Harb. Symp. Quant. Biol*. **58**, 799-805.

Tokuyasu, K. T. (1980). Immunocytochemistry in ultra-thin frozen sections. *Histochem. J*. **12**, 381-403.

Tooze, J., Hollingshead, M., Hensel, G., Kern, H. F. and Hoflack, B. (1991). Regulated secretion of mature cathepsin B from rat exocrine pancreatic cells. *Eur. J. Cell Biol*. **56**, 187-200.

Walker, L. J., Robson, C. N., Black, E., Gillespie, D. and Hickson, I. D. (1993). Identification of residues in human DNA repair enzyme HAP1 (Ref-1) that are essential for redox regulation of Jun DNA binding. *Mol. Cell. Biol*. **13**, 5370-5376.

Wansink, D. G., Schul, W., van der Kraan, I., van Steensel, B., van Driel, R. and de Jong, L. (1993). Fluorescent labelling of nascent RNA reveals transcription by RNA polymerase II in domains scattered throughout the nucleus. *J. Cell Biol*. **122**, 283-293.

Wansink, D. G. (1994). Transcription by RNA polymerase II and nuclear architecture. Thesis Universiteit van Amsterdam.

Wansink, D. G., Nelissen, R. L. and de Jong, L. (1994). In vitro splicing of pre-mRNA containing bromouridine. *Mol. Biol. Rep*. **19**, 109-113.

Williams, M. (1977). Stereological techniques. *Pract. Meth. Electron Microsc*. **6**, 6-80.

(Received 19 January 1996 - Accepted 15 March 1996)